

TESTING THE VACUUM OSCILLATION AND THE MSW
SOLUTIONS OF THE SOLAR NEUTRINO PROBLEM

P. I. Krastev*

*Institute of Field Physics, Department of Physics and Astronomy,
The University of North Carolina, Chapel Hill, NC 27599-3255,*

S.T. Petcov*

*Scuola Internazionale Superiore di Studi Avanzati, and Istituto
Nazionale di Fizica Nucleare, Sezione di Trieste, I-34013 Trieste, Italy*

Abstract

Solar model independent tests of the vacuum oscillation and MSW solutions of the solar neutrino problem are considered. Detailed predictions for time (seasonal) variations of the signals in the future solar neutrino detectors (SNO, Super Kamiokande, BOREXINO, HELLAZ), if solar neutrinos take part in vacuum oscillations, are given. Results on the distortions of the spectra of ${}^8\text{B}$ neutrinos, and of e^- from the reaction $\nu + e^- \rightarrow \nu + e^-$ induced by ${}^8\text{B}$ neutrinos, in the cases of vacuum oscillations or MSW transitions are presented for a large number of values of the relevant parameters. The possibilities to distinguish between the vacuum oscillation, the MSW adiabatic, and the MSW nonadiabatic transitions (solutions) in the future solar neutrino experiments are discussed.

*Permanent address: Institute of Nuclear Research and Nuclear Energy, Bulgarian Academy of Sciences, BG-1784 Sofia, Bulgaria.



1. INTRODUCTION

With the publication in 1991 and 1992 of the results of the Ga-Ge solar neutrino experiments [1,2] it became clear that the data from the first generation of solar neutrino detectors will not be sufficient to resolve the solar neutrino problem [3-6] which has been with us for more than 20 years. If the latest data provided by the pioneer Davis et al. [3], Kamiokande [7], SAGE [1] and GALLEX [2] experiments are correct, an astrophysical explanation of the solar neutrino deficit seems unlikely at present [8] (for a recent discussion see [9] and [10]). At the same time, the current solar neutrino observations admit several rather different neutrino physics interpretations which require the existence of unconventional neutrino intrinsic properties (mass, mixing, magnetic moment) and/or couplings (e.g., flavour changing neutral current (FCNC) interactions). These include: i) oscillations in vacuum [11] of the solar ν_e into different weak eigenstate neutrinos (ν_μ and/or ν_τ , and/or sterile neutrinos, ν_s) on the way from the surface of the Sun to the Earth [12]¹, ii) MSW transitions [13] $\nu_e \rightarrow \nu_{\mu(\tau)}$, and/or $\nu_e \rightarrow \nu_s$, while the solar neutrinos propagate from the central part to the surface of the Sun [14]², iii) solar ν_e resonant spin or spin-flavour precession (RSFP) [16] in the magnetic field of the Sun [17], and iv) matter-enhanced transitions, for instance $\nu_e \rightarrow \nu_\tau$, in the Sun, induced by FCNC interactions of the solar ν_e with the particles forming the solar matter [18,19] (these transitions can take place even in the case of absence of lepton mixing in vacuum and massless neutrinos [18])³. Although the experiments of Davis et al., Kamiokande, SAGE and GALLEX will continue to run for at least few more years and the

¹For earlier discussions see, e.g., the references quoted in [12].

²The MSW solution has been studied by many authors before and after the publication of the results of the two Ga-Ge experiments: see, e.g., refs. [2,15] and the references quoted in [2,14,15].

³The solar neutrino decay hypothesis [20] is disfavoured [21], while mechanisms leading to universal suppression of the fluxes of ^8B , ^7Be , pp, etc. neutrinos due to $\nu_e \rightarrow \nu_s$ transitions are ruled out, by the current solar neutrino data, if one uses the standard solar model (SSM) predictions of refs. [5,6] in the relevant analyses.

accuracy of the data they provided will improve, no substantial changes of the latter are expected ⁴ and no qualitatively new data will be available before solar neutrino detectors of the second generation - SNO [22], Super Kamiokande [23], BOREXINO [24], ICARUS [25], and HELLAZ [26], become operational in the second half of the 90-ies ⁵. Our hopes for finding the cause of the solar neutrino deficit and for getting more precise information about the physical conditions in the central part of the Sun, where the neutrinos are being produced, are now associated with these future experiments.

In the present article we continue the studies [14,27] of the possible solar model independent tests of the vacuum oscillation and the MSW solutions of the solar neutrino problem. The importance of these tests is difficult to overestimate given the fact that the solar model predictions for the ⁸B neutrino flux may have rather large uncertainties. We present results on the specific seasonal time variations of the signals in the future solar neutrino experiments (SNO, Super Kamiokande, BOREXINO, HELLAZ), predicted if the solar neutrino deficit is caused by vacuum oscillations of solar neutrinos. We give also detailed predictions for the distortions of the spectra of ⁸B neutrinos, and of e^- from the reaction $\nu + e^- \rightarrow \nu + e^-$ caused by the ⁸B neutrinos, in the cases of the vacuum oscillation and the MSW solutions. Neither seasonal time variations (apart from the standard $\sim 7\%$ geometrical one), nor substantial distortions of the spectra of the ⁸B, pp and CNO neutrinos (greater than $\sim 10^{-3}$ E, E being the neutrino energy) are predicted to arise due to the specific physical conditions in the interior of the Sun [28]. The possibilities to distinguish between the vacuum oscillation, the

⁴A priori, one cannot totally rule out the possibility of surprises in the next few years. The planned calibrations of the GALLEX and SAGE detectors will be crucial for the conclusive determination of the characteristics of the solar neutrino flux inferred from the current data.

⁵Two of these detectors - SNO and Super Kamiokande, are under construction, BOREXINO and ICARUS are at the stage of prototype construction and/or testing, and the possibility to build HELLAZ is being studied.

MSW adiabatic, and the MSW nonadiabatic solutions of the solar neutrino problem using the data from the future SNO and Super Kamiokande experiments are discussed ⁶. Updated results on the MSW solution of the solar neutrino problem are also given.

2. VACUUM OSCILLATIONS OF SOLAR NEUTRINOS: PREDICTED SEASONAL VARIATION EFFECTS AND SPECTRA DISTORTIONS

The two-neutrino vacuum oscillation solution of the solar neutrino problem has been re-analyzed recently [30] using the latest data from all currently operating neutrino experiments (Homestake, Kamiokande III, GALLEX and SAGE). The analysis was based on the predictions of the solar model of Bahcall and Pinsonneault [5]. It was found that the two-neutrino oscillations involving the ν_e and an active neutrino, $\nu_e \leftrightarrow \nu_{\mu(\tau)}$, provide a not very good (but acceptable) quality of the χ^2 -fit to the mean event rate solar neutrino data, while the oscillations into sterile neutrino ν_s , $\nu_e \leftrightarrow \nu_s$, give a poor fit of the data: the $\nu_e \leftrightarrow \nu_{\mu(\tau)}$ oscillations are ruled out at 90 % C.L., but are acceptable at 95 % C.L., while the $\nu_e \leftrightarrow \nu_s$ oscillations are ruled out at 99 % C.L. The results are rather different if one uses the data available from each particular run of measurement of the Homestake, Kamiokande II, GALLEX and SAGE collaboration in the χ^2 -analysis (for details see ref. [30]). Both the $\nu_e \leftrightarrow \nu_{\mu(\tau)}$ and $\nu_e \leftrightarrow \nu_s$ oscillation hypotheses give good fits to the run-by-run solar neutrino data, being acceptable even at 68 % C.L. The regions of values of the two parameters, Δm^2 and $\sin^2 2\theta$, characterizing the two-neutrino oscillations of the solar ν_e , which are allowed (at 90 % C.L.) by the run-by-run data, lie in the following narrow intervals [30]:

$$\nu_e \leftrightarrow \nu_{\mu(\tau)} : \quad 5.7 \times 10^{-11} \text{eV}^2 \lesssim \Delta m^2 \lesssim 1.1 \times 10^{-10} \text{eV}^2, \quad (1a)$$

$$\sin^2 2\theta \gtrsim 0.75, \quad (1b)$$

⁶For alternative solar model independent tests of these solutions, based on the future SNO and Super Kamiokande data see refs. [29].

and

$$\nu_e \leftrightarrow \nu_s : \quad 5.0 \times 10^{-11} \text{eV}^2 \lesssim \Delta m^2 \lesssim 6.6 \times 10^{-11} \text{eV}^2, \quad (2a)$$

$$\sin^2 2\theta \gtrsim 0.8. \quad (2b)$$

2.1 Seasonal Variations of Signals

The probability that a solar electron neutrino with energy E will not change into $\nu_{\mu(\tau)}$ (or ν_s) on its way to the Earth when $\nu_e \leftrightarrow \nu_{\mu(\tau)}$ ($\nu_e \leftrightarrow \nu_s$) oscillations take place, has the form:

$$P(\nu_e \rightarrow \nu_e; R(t), E) = 1 - \frac{1}{2} \sin^2 2\theta \left[1 - \cos 2\pi \frac{R(t)}{L_\nu} \right], \quad (3)$$

where $L_\nu = 4\pi E / \Delta m^2$ is the oscillation length in vacuum,

$$R(t) = R_0 \left[1 - \epsilon \cos 2\pi \frac{t}{T} \right], \quad (4)$$

is the Sun–Earth distance at time t of the year ($T = 365$ days), $R_0 = 1.496 \times 10^8$ km and $\epsilon = 0.0167$ being the mean Sun–Earth distance and the ellipticity of the Earth orbit around the Sun.

For $E \simeq 1$ MeV and the values of Δm^2 from the intervals (1a) and (1b) one has: $L_\nu \simeq 2\pi(2\epsilon R_0)$, where $2\epsilon R_0$ is the variation of the Sun–Earth distance in the period December – June. This implies that if solar neutrinos take part in vacuum oscillations, the flux of solar neutrinos will exhibit seasonal variations⁷. The magnitude of the time variations depends, in particular, on the energy of solar neutrinos and will be different for the ${}^8\text{B}$, ${}^7\text{Be}$, pp, pep and the CNO neutrinos. Obviously, if the integration over the neutrino energy renders the oscillating term in the expression for $P(\nu_e \rightarrow \nu_e; R(t), E)$ negligible (as is the case of pp neutrinos [12]), the energy integrated observables will not exhibit seasonal (time) variations.

⁷The possibility of seasonal variations of the flux of solar neutrinos when the latter take part in oscillations in vacuum was indicated first by B.Ya. Pomeranchuk (see, e.g., ref. [31]).

We have depicted in Figs. 1 and 2 the expected time variation of the ratio of the predicted signals (event rates) due to the ^8B , pp , ^7Be and pep neutrinos in the case of (two-neutrino) oscillations of solar neutrinos, to the ones in the absence of oscillations. The results shown in these figures are valid for experiments detecting the solar neutrinos via the $\nu - e^-$ elastic scattering reaction (Super Kamiokande, BOREXINO, HELLAZ, etc.). The electron kinetic energy detection threshold was taken in the calculations of the signals due to the ^8B , the pp , the ^7Be and pep neutrinos to be 5 MeV, 0.1 MeV, and 0 MeV, respectively; the possible effects of the detectors efficiencies and finite electron energy resolution were not included in the calculations (we leave it to our colleagues-experimentalists to take into account these effects in accordance with the specific characteristics of their respective detectors). Electrons with kinetic energy $T_e \gtrsim 5$ MeV will be detected in the Super Kamiokande experiment. The HELLAZ detector is planned to be sensitive to e^- (from the pp neutrino induced reaction) with $T_e \gtrsim 0.1$ MeV. As for the BOREXINO detector in which $\sim 90\%$ of the event rate is predicted to be generated by the 0.862 MeV ^7Be neutrinos, it is expected that the signal to background ratio will allow one to extract the ^7Be neutrino signal for e^- with kinetic energy in the interval $0.25 \text{ MeV} \lesssim T_e \lesssim 0.66 \text{ MeV}$. We have checked that reducing the interval $0 \leq T_e \lesssim 0.66 \text{ MeV}$ used in our calculations to the one reflecting the currently envisaged detection capabilities of BOREXINO has no observable effect on the results (the two $^7\text{Be}(862)$ curves, corresponding to the two different intervals of integration would be indistinguishable if both were plotted in Figs. 1 and 2).

In the calculations of the signals (event rates) in the case of vacuum oscillations we have taken into account also the standard $R^{-2}(t)$ dependence of the values of the different solar neutrino flux components at the Earth surface. Finally, the SSM predicted event rates (signals) have been obtained by dividing by T the one year total number of events calculated within the SSM [5] (assuming 100% detection efficiency). Thus, in the absence of vacuum oscillations the plotted (theoretical) ratios will change from $(1 - \epsilon)^{-2}$ in December to $(1 + \epsilon)^{-2}$ in June, while the ratio of measured to the SSM predicted [5] signals will vary from $A(1 - \epsilon)^{-2}$ to $A(1 + \epsilon)^{-2}$, where A is a constant which can be different for the different

(pp, ${}^7\text{Be}$, ${}^8\text{B}$, and pep neutrino induced) signals ($A = 1$ if the SSM prediction [5] for the flux of the corresponding neutrinos (pp, and/or ${}^7\text{Be}$, and/or ${}^8\text{B}$, and/or pep) is correct).

The results shown in Figs. 1 and Figs. 2a-2d correspond to solar ν_e oscillations into active neutrino, $\nu_e \leftrightarrow \nu_{\mu(\tau)}$, while in Fig. 2e and Fig. 2f we have depicted results in the case of oscillations into sterile neutrino, $\nu_e \leftrightarrow \nu_s$.

As was indicated on the basis of few numerical examples in [14,27], the most dramatic seasonal variations are predicted to be exhibited by the signals due to the monochromatic ${}^7\text{Be}$ and pep neutrinos. Typically, the differences between the signals in December and June are the largest. However, as was noted in [14], for certain values of the parameter Δm^2 the signals in December (or June) and March (or September) differ most (see, e.g., Figs. 1c, 1d and 2f). Figs. 1 and 2 demonstrate also that the predicted magnitude and explicit form of the time variations of the ${}^7\text{Be}$ and pep neutrino induced event rates in the $\nu - e^-$ elastic scattering experiments are extremely sensitive to the value of Δm^2 and change drastically even for relatively small variations of this parameter.

Since the pp neutrinos have a rather low energy ($E \leq 0.42$ MeV), for most of the values of Δm^2 from the intervals (1a) and (2a) the inequality $2\pi R_o \gg L_\nu$ holds. As a consequence, the integration over the recoil e^- energy in the calculations of the pp neutrino induced signals renders the oscillation term in the probability (3) negligible [12]. Therefore the predicted seasonal change of the energy integrated signals due to the pp neutrinos in the $\nu - e^-$ scattering experiments coincides with the standard 7% geometrical one (Figs. 1, 2a-2c, and 2e), except for values of $\Delta m^2 \approx 5 \times 10^{-11} \text{ eV}^2$, for which the vacuum oscillations lead to rather small deviations from it (Figs. 2c and 2f).

The seasonal changes of the signal due to the ${}^8\text{B}$ neutrinos do not exceed approximately 15% [14]. Such variations are not detectable in the currently running experiments. However, the high statistics future solar neutrino experiments Super Kamiokande, SNO, and ICARUS are envisaged to accumulate (between 3000 and 4000 events per year) will allow to detect even rather small (few percent) differences between the signals in December and June. For Super Kamiokande (ICARUS) and SNO detectors the effect of time variations is shown

separately in Figs. 3a (3b), 3d (3e), and in Figs. 3c and 3f, respectively, using a different normalization of the signals and a proper scale. The predictions for the Super Kamiokande detector depicted in Figs. 3a (3d) and 3b (3e) differ in the value of the neutrino threshold energy, E_{th} , used in the calculations (see further): $E_{th} = 5$ MeV and $E_{th} = 7.5$ MeV, respectively. The smaller magnitude of the effect in comparison with that in the case of the signals, generated by the monoenergetic ${}^7\text{Be}$ and pep neutrinos, is not difficult to understand qualitatively. The Super Kamiokande and SNO experiments will be sensitive only to ${}^8\text{B}$ neutrinos having relatively high energies ($E \geq 5$ MeV and $E \geq 6.44$ MeV) which exceed at least by a factor of 6 the energy of the dominant (0.862 MeV) component of the ${}^7\text{Be}$ neutrino flux. For these energies and the values of Δm^2 from the intervals (1a) and (1b) one has: $2\pi(\epsilon R_0/L_\nu) \leq 0.14$. As it follows from eqs. (3) and (4), under this condition the seasonal changes of the probability $P(\nu_e \rightarrow \nu_e; R(t), E)$ are proportional to, and do not exceed, the ratio $2\pi(\epsilon R_0/L_\nu)$ and, therefore, cannot be large. The integration over the neutrino energy reduces further the magnitude of the effect of interest.

The solid, dotted, dashed, long-dashed, dash-dotted, and long-dash-dotted lines in Figs. 3a, 3b and 3c (Figs. 3d, 3e and 3f) represent results for the values of Δm^2 and $\sin^2 2\theta$ for which Figs. 1a, 1b,..., 1f (Figs. 2a, 2b,..., 2f) have been obtained. The normalization of the signals shown graphically in Figs. 3 is chosen in such a way as to avoid any dependence on the prediction for the total flux of ${}^8\text{B}$ neutrinos, and thus on the solar models. Namely, for given Δm^2 and $\sin^2 2\theta$ the calculated event rate at time t of the year in the case of vacuum oscillations, $dN_{ev}(\Delta m^2, \theta, E_{th}; t)/dt$, is divided by the quantity $dN_{ev}^0(t)/dt = N_{ev}(\Delta m^2, \theta, E_{th}; 1y) T^{-1}(R_0/R(t))^2$, where $N_{ev}(\Delta m^2, \theta, E_{th}; 1y)$ is the predicted total number of events per year provided ${}^8\text{B}$ neutrinos undergo vacuum oscillations with the chosen values of the parameters Δm^2 and $\sin^2 2\theta$, and the ratio

$$R_{var}(\Delta m^2, \theta, E_{th}; t) = \frac{dN_{ev}(\Delta m^2, \theta, E_{th}; t)/dt}{dN_{ev}^0(t)/dt} = T \frac{R^2(t)}{R_0^2} \frac{dN_{ev}(\Delta m^2, \theta, E_{th}; t)/dt}{N_{ev}(\Delta m^2, \theta, E_{th}; 1y)}, \quad (5)$$

is plotted in Figs. 3. For the SNO detector we have:

$$\frac{dN_{ev}(\Delta m^2, \theta, E_{th}; t)}{dt} = \frac{1}{R^2(t)} \int_{E_{th}}^{14.4 \text{ MeV}} F^{\text{SSM}} n(E) P(\nu_e \rightarrow \nu_e; R(t), E) \sigma(\nu_e d \rightarrow e^- pp) dE, \quad (6)$$

$$N_{ev}(\Delta m^2, \theta, E_{th}; 1 y) = \int_0^T \frac{dN_{ev}(\Delta m^2, \theta, E_{th}; t)}{dt} dt, \quad (7)$$

where $F^{\text{SSM}}/R^2(t)$ is the predicted total flux of ${}^8\text{B}$ neutrinos at the Earth surface at time t of the year, $n(E)$ is the normalized to 1 spectrum of ${}^8\text{B}$ neutrinos, $\int_0^{14.4 \text{ MeV}} n(E) dE = 1$, $E_{th} = 6.44 \text{ MeV}$, and $\sigma(\nu_e d \rightarrow e^- pp)$ is the cross-section of the charged current reaction $\nu_e + d \rightarrow e^- + p + p$ by which the solar neutrinos will be detected in the SNO experiment. Obviously, expression (6) corresponds to ideal detection conditions; for the comparison of the theoretical predictions with the future SNO data it has to be modified by taking into account the neutrino energy resolution function, the detection efficiency, etc. of the SNO detector. The expression for the predicted event rate in the Super Kamiokande detector can be obtained from eq. (6) by replacing $\sigma(\nu_e d \rightarrow e^- pp)$ with the cross-section $\sigma(\nu_e e^- \rightarrow \nu_e e^-)$ of the reaction $\nu_e + e^- \rightarrow \nu_e + e^-$, and by using an appropriate value for E_{th} ; in the case of $\nu_e \leftrightarrow \nu_{\mu(\tau)}$ oscillations the probability $P(\nu_e \rightarrow \nu_e; R(t), E)$ must be substituted with

$$r_\nu + (1 - r_\nu) P(\nu_e \rightarrow \nu_e; R(t), E), \quad (8)$$

where $r_\nu = \sigma(\nu_\mu e^- \rightarrow \nu_\mu e^-) / \sigma(\nu_e e^- \rightarrow \nu_e e^-) \cong \frac{1}{6}$.

It is not difficult to convince oneself that $dN(t)_{ev}^0/dt$ is the event rate at time t of the year if the total number of events per year is $N_{ev}(\Delta m^2, \theta, E_{th}; 1 y)$ and the relevant signal does not exhibit any additional time dependence, except for the standard $R^{-2}(t)$ geometrical one. The ratio (5), evidently, is independent of the value of F^{SSM} and thus is solar model independent. The comparison of the predictions presented graphically in Figs. 3 with the data will be straightforward: as input one needs only the experimentally measured mean event rate for a given interval of time (one month, say), and the total number of events observed per year; the latter will provide the value of $N_{ev}(\Delta m^2, \theta, E_{th}; 1 y)$. All the other quantities entering into the ratio (5), T , R_0 and $R(t)$, are known with a high precision. In

the absence of vacuum oscillations the ratios of signals (5) plotted in Figs. 3 will be equal to 1.

We shall obtain next an approximate but sufficiently accurate and rather simple analytic expression for the time variation observable (5), exhibiting its time dependence explicitly. For $\epsilon = 0.0167 \ll 1$ and $2\pi(\epsilon R_0/L_\nu) \leq 0.14 \ll 1$, the quantity $2\pi(\epsilon R_0/L_\nu) \cos(2\pi t/T)$ entering into the formula for the probability $P(\nu_e \rightarrow \nu_e; R(t), E)$, can be used as a small expansion parameter together with $\epsilon \cos(2\pi \frac{t}{T})$. Expressing the oscillating term in $P(\nu_e \rightarrow \nu_e; R(t), E)$ as a power series in $2\pi(\epsilon R_0/L_\nu) \cos(2\pi t/T)$, and $R(t)$ as a power series in $\epsilon \cos(2\pi \frac{t}{T})$, it is easy to show that the leading correction in $N_{\nu_e}(\Delta m^2, \theta, E_{th}; 1 y)$ due to the ellipticity ϵ is proportional to ϵ^2 and does not exceed 5×10^{-3} . Thus, up to corrections $\sim 5 \times 10^{-3}$, the quantity $N_{\nu_e}(\Delta m^2, \theta, E_{th}; 1 y)$ does not depend on ϵ and can be obtained by setting ϵ to 0 in eqs. (6) and (7). Using this fact, and keeping in (6) only the terms up to the second order in $2\pi(\epsilon R_0/L_\nu) \cos(2\pi t/T)$ in the expansion of $P(\nu_e \rightarrow \nu_e; R(t), E)$, one arrives at the following result for the observable $R_{\text{var}}(\Delta m^2, \theta, E_{th}; t)$ for the SNO detector:

$$R_{\text{var}}^{\text{SNO}}(\Delta m^2, \theta, E_{th}; t) = 1 + \epsilon \cos(2\pi \frac{t}{T}) \sin^2 2\theta K^{\text{SNO}}(\Delta m^2, \theta, E_{th}), \quad (9)$$

where

$$K^{\text{SNO}}(\Delta m^2, \theta, E_{th}) = \frac{\int_{E_{th}}^{14.4 \text{ MeV}} dE x(\sin 2x - x \cos 2x \epsilon \cos 2\pi \frac{t}{T}) n(E) \sigma(\nu_e d \rightarrow e^- pp)}{\int_{E_{th}}^{14.4 \text{ MeV}} dE P(\nu_e \rightarrow \nu_e; R_0, E) n(E) \sigma(\nu_e d \rightarrow e^- pp)} + O((2x)^3), \quad (10)$$

and $x = \epsilon \pi R_0/L_\nu \leq 0.07$. The corresponding expression for the time variation observable for the Super Kamiokande detector, $R_{\text{var}}^{\text{SK}}(\Delta m^2, \theta, E_{th}; t)$, can be obtained formally from eqs. (9) and (10) by replacing in eq. (10) the probability $P(\nu_e \rightarrow \nu_e; R(t), E)$ by $[r_\nu + (1 - r_\nu) P(\nu_e \rightarrow \nu_e; R(t), E)]$, $\sigma(\nu_e d \rightarrow e^- pp)$ with $\sigma(\nu_e e^- \rightarrow \nu_e e^-)$, by changing the value of E_{th} , and by multiplying the numerator in eq. (10) by the factor $(1 - r_\nu)$. Let us note that the effect of the time dependence of $K^{\text{SNO(SK)}}(\Delta m^2, \theta, E_{th})$ on $R_{\text{var}}^{\text{SNO(SK)}}(\Delta m^2, \theta, E_{th}; t)$ is beyond the sensitivity of the next generation of experiments.

Few comments concerning the results shown in Figs. 3 are in order. All (correspondingly

normalized) signals are equal to 1 at $t = \frac{1}{4}T$ and $t = \frac{3}{4}T$, in accordance with eqs. (9) and (10). As Figs. 3 indicate, the predicted amplitude of the time variations of the signal in the SNO detector is typically (but not always, e.g., compare the dashed and the long-dashed lines in Figs. 3a and 3c) larger than that in the Super Kamiokande detector. The difference in the magnitude of the signal time variations in the two detectors is a consequence of i) the difference in the minimal ${}^8\text{B}$ neutrino energy the two detectors are planned to be sensitive to (6.44 MeV and 5 MeV), ii) the specific neutrino energy dependence of $P(\nu_e \rightarrow \nu_e; R(t), E)$ in December and June, iii) the difference in the E -dependence of the cross-sections $\sigma(\nu_e d \rightarrow e^- pp)$ and $\sigma(\nu_e e^- \rightarrow \nu_e e^-)$, and in the case of $\nu_e \leftrightarrow \nu_{\mu(\tau)}$ oscillations iv) the probability $P(\nu_e \rightarrow \nu_e; R(t), E)$ entering into the expression for the predicted signals in SNO and Super Kamiokande detectors with different coefficients (see eqs. (6) and (8)): 1 and approximately $\frac{5}{8}$, respectively. These differences can lead even to a strong anticorrelation between the signals in SNO and Super Kamiokande experiments, as in the case of $\Delta m^2 = 6.9 \times 10^{-11} \text{ eV}^2$ and $\sin^2 2\theta = 0.9$ (the solid lines in Figs. 3d and 3f).

If $|K^{\text{SNO(SK)}}(\Delta m^2, \theta, E_{th})| \ll 1$ for certain values of Δm^2 and $\sin^2 2\theta$, one has $R_{\text{var}}^{\text{SNO(SK)}}(\Delta m^2, \theta, E_{th}; t) = 1 + O(10^{-3})$, and the time variation effects will not be observable in SNO (Super Kamiokande) experiment in spite of vacuum oscillations of ${}^8\text{B}$ neutrinos. Such is practically the case with the signal in the Super Kamiokande detector for $E_{th} = 5 \text{ MeV}$, $\Delta m^2 = 6.3 \times 10^{-11} \text{ eV}^2$ and $\sin^2 2\theta = 0.85$ (see Figs. 1e and 2e and the dash-dotted lines in Figs. 3a and 3d). Fortunately, our results show that the indicated possibility is never realized both for the signals in the Super Kamiokande and the SNO detectors (compare the dash-dotted lines in Figs. 3a, 3d and in Figs. 3c and 3e). Moreover, it can take place either for the event rate in the Super Kamiokande detector measured with $E_{th} = 5 \text{ MeV}$, or for the event rate obtained with $E_{th} = 7.5 \text{ MeV}$ (the long-dashed line in Fig. 3b), but not for both event rates (compare the dash-dotted lines in Figs. 3a, 3d and in Figs. 3b, 3e, and the long-dashed lines in Figs. 3b and 3a).

In certain cases the magnitude and the pattern of the time variation of the signal in the Super Kamiokande detector is very sensitive to the increase of the threshold neutrino

energy from $E_{th} = 5$ MeV to $E_{th} = (7 - 8)$ MeV. This is illustrated in Figs. 3b and 3e, where the results of the calculations of the ratio of signals (5) for the same values of Δm^2 and $\sin^2 2\theta$, for which Figs. 3a and 3d were obtained, but with $E_{th} = 7.5$ MeV (instead of $E_{th} = 5$ MeV), are presented. We see, in particular, that for $\Delta m^2 = 6.9 \times 10^{-11}$ eV² and $\sin^2 2\theta = 0.9$ the pattern of the time variations has changed completely with the change of E_{th} : the maximum of the ratio (5) is now in December rather than in June, and the predicted variations of the signals in the SNO and Super Kamiokande detectors are correlated (rather than anticorrelated). Depending on the value of Δm^2 (and $\sin^2 2\theta$), the change of E_{th} from 5 MeV to 7.5 MeV can increase, or diminish the amplitude of the variations (compare, e.g., the solid, dotted, dash-dotted, and long-dash-dotted lines in Figs. 3a and 3b, as well as the dashed and long-dashed lines in the same two figures); for some values of Δm^2 and $\sin^2 2\theta$ the increase is quite substantial. We have not studied the effect of change of E_{th} on the time variation of the signal in the SNO detector. However, one can expect on the basis of the above results that for certain values of Δm^2 and $\sin^2 2\theta$ it can be dramatic.

It is interesting to note also [14,27] that for certain values of the parameters Δm^2 and $\sin^2 2\theta$ the seasonal change of the ⁸B neutrino induced signals, associated with the vacuum oscillations, can compensate partially or completely the standard 7% geometrical one and in the second case the event rate $dN_{ev}(\Delta m^2, \theta, E_{th}; t)/dt$ will be constant in time (see Figs. 1a-1d and 2a and the corresponding solid, dotted, dashed and long-dashed lines in Fig. 3a, the dotted line in Fig. 3b, the dashed and long-dashed lines in Fig. 3c, as well as the solid line in Fig. 3d); it can even lead to an increase of the event rate $dN_{ev}(\Delta m^2, \theta, E_{th}; t)/dt$ from December to June ⁸ (see the solid line in Fig. 3b and the solid and dotted lines in Fig. 3c). Note that due to the specific normalization chosen by us a constant event rate

⁸In the case of the monoenergetic ⁷Be and pep neutrinos even a dramatic increase of the corresponding signals from December to June due to the vacuum oscillations is possible (as can be seen in Figs. 1 and 2).

will correspond to an increase of the ratio (5) plotted in Figs. 3 from the value $(1 - 2\epsilon)$ in December to the value $(1 + 2\epsilon)$ in June; an increase of the event rate from December to June corresponds to an increase of the ratio (5) from a value smaller than $(1 - 2\epsilon)$ in December to a value greater than $(1 + 2\epsilon)$ in June (see the solid line in Fig. 3b and the solid and dotted lines in Figs. 3c). Thus, a non-observation of the 7% change of the ^8B neutrino induced event rate (constant rate), or a registration of an increase of the rate, in the period from December to June in SNO and/or Super Kamiokande detector would be a strong evidence that solar neutrinos take part in vacuum oscillations. Note that, as is clear from Figs. 3, for given Δm^2 and $\sin^2 2\theta$ the compensation (partial or complete) of the standard 7% seasonal variation can take place either for SNO or for Super Kamiokande signals, but not for the signals in both detectors. Furthermore, in the case of the signal in the Super Kamiokande detector such a compensation does not hold both for $E_{th} = 5$ MeV and for $E_{th} = 7.5$ MeV.

2.2 Spectra Deformations

If solar neutrinos take part in vacuum oscillations, the shapes of the spectra of the ^8B , pp, and the CNO neutrino fluxes at the Earth surface will differ from their standard forms. The corresponding spectra deformations will reflect the specific and relatively strong dependence of the oscillation probability $P(\nu_e \rightarrow \nu_e; R(t), E)$, eq. (3), on the neutrino energy E . The change of the solar neutrino spectrum will lead also to a change in the spectrum of the final state electrons in the $\nu - e^-$ elastic scattering reaction induced by the solar neutrinos.

The deformation of the (average) spectrum of ^8B neutrinos ⁹ for the same 12 values of

⁹The spectra under discussion will also exhibit relatively small seasonal variations if solar neutrinos undergo vacuum oscillations. Here we have in mind the average spectrum which will be determined experimentally from data collected during a period of k years, $k = 1, 2, 3, \dots$. The relative magnitude of the correction due to the seasonal variations in the average spectrum of ^8B neutrinos is not greater than $\sim 5 \times 10^{-3}$, while the relative difference between the spectra in December and June does not exceed 14%.

the parameters Δm^2 and $\sin^2 2\theta$, for which Figs. 1a-1f, 3a-3c and Figs. 2a-2f, 3d-3f have been obtained, are shown respectively in Fig. 4a and Fig. 4b. Each (average) spectrum, $d\Phi_B(\Delta m^2, \theta, E)/dE$, to be determined from data collected by the SNO experiment over a period of k years,

$$\begin{aligned} \frac{d\Phi_B(\Delta m^2, \theta, E)}{dE} &= \frac{1}{kT} \frac{1}{\sigma(\nu_e d \rightarrow e^- pp)} \frac{dN_{\nu_e}(\Delta m^2, \theta, E; k)}{dE} = \\ &= \frac{F^{\text{SSM}}}{R_0^2} n(E) P(\nu_e \rightarrow \nu_e; R_0, E), \end{aligned} \quad (11)$$

$dN_{\nu_e}(\Delta m^2, \theta, E; k)/dE$ being the total number of events induced by ${}^8\text{B}$ neutrinos with energy E in $k=1,2,3,\dots$ years, while the last term in eq. (11) represents the theoretical expression for the spectrum in the case of vacuum oscillations, is divided by the (average) SSM spectrum,

$$\frac{d\Phi_B^{\text{SSM}}(E)}{dE} = \frac{F^{\text{SSM}}}{R_0^2} n(E), \quad (12)$$

predicted in the absence of oscillations. To avoid the dependence on the SSM prediction for the total flux of ${}^8\text{B}$ neutrinos this ratio of spectra,

$$R_{\text{sp}}^{\text{SNO}}(\Delta m^2, \theta, E) = \frac{d\Phi_B(\Delta m^2, \theta, E)/dE}{d\Phi_B^{\text{SSM}}(E)/dE}, \quad (13)$$

is further normalized to the value of the ratio at $E = 10$ MeV, and the double ratio

$$\begin{aligned} \frac{R_{\text{sp}}^{\text{SNO}}(\Delta m^2, \theta, E)}{R_{\text{sp}}^{\text{SNO}}(\Delta m^2, \theta, 10 \text{ MeV})} &= \frac{(n(E) \sigma(\nu_e d \rightarrow e^- pp))_{E=10 \text{ MeV}}}{n(E) \sigma(\nu_e d \rightarrow e^- pp)} \frac{dN_{\nu_e}(\Delta m^2, \theta, E; k)/dE}{dN_{\nu_e}(\Delta m^2, \theta, 10 \text{ MeV}; k)/dE} = \\ &= \frac{P(\nu_e \rightarrow \nu_e; R_0, E)}{P(\nu_e \rightarrow \nu_e; R_0, E = 10 \text{ MeV})}, \end{aligned} \quad (14)$$

is plotted in Figs. 4a and 4b. Thus, in the case of absence of deformations the ratio of spectra depicted will be constant (i.e., neutrino energy independent) and equal to 1¹⁰. Note

¹⁰The absolute deformations of the spectra of the ${}^8\text{B}$ and pp neutrinos in the case of $\nu_e \leftrightarrow \nu_{\mu(\tau)}$ (or $\nu_e \leftrightarrow \nu_s$) oscillations, and for the SSM predictions of ref. [5] have been shown in ref. [27] for four pairs of values of the parameters Δm^2 and $\sin^2 2\theta$, namely, for $(\Delta m^2[\text{eV}^2]; \sin^2 2\theta) = (1.1 \times 10^{-10}; 1.0), (7.9 \times 10^{-11}; 0.8), (6.3 \times 10^{-11}; 0.8), (5.5 \times 10^{-11}; 1.0)$.

that this would be valid both for a constant reduction of the spectrum of the flux (and therefore of the total flux) of ${}^8\text{B}$ neutrinos by a certain (energy independent) factor, and if there is no reduction at all and the flux coincides with the predicted one.

The changes of the (average) spectrum of the final state e^- in the $\nu-e^-$ elastic scattering reaction induced by the ${}^8\text{B}$ neutrinos in the cases of $\nu_e \leftrightarrow \nu_{\mu(\tau)}$ ¹¹, and of $\nu_e \leftrightarrow \nu_s$ oscillations are shown respectively in Fig. 5a, Fig. 5b (curves labelled 1-4), and in Fig. 5b (curves labelled 5 and 6), for the same 12 values of Δm^2 and $\sin^2 2\theta$ for which Figs. 1, 2, 3 and Figs. 4a, 4b have been obtained. The e^- kinetic energy range chosen ($5 \text{ MeV} \leq T_e \leq 14 \text{ MeV}$) coincides with the one to which the Super Kamiokande detector is planned to be sensitive. The recoil-electron spectra depicted in Figs. 5a and 5b are normalized in the same way as the spectra shown in Figs. 4a and 4b¹², i.e., the following double ratio is plotted in Figs. 5a and 5b:

$$\frac{R_{\text{sp}}^{\text{SK}}(\Delta m^2, \theta, T_e)}{R_{\text{sp}}^{\text{SK}}(\Delta m^2, \theta, 10 \text{ MeV})} = w(T_e) \frac{dN_{\text{ev}}(\Delta m^2, \theta, T_e; k)/dT_e}{dN_{\text{ev}}(\Delta m^2, \theta, 10 \text{ MeV}; k)/dT_e} =$$

$$= w(T_e) \frac{\int_{T_e(1+\frac{m_e}{2T_e})}^{14.4 \text{ MeV}} n(E) (r'_\nu + (1 - r'_\nu)P(\nu_e \rightarrow \nu_e; R_0, E)) (d\sigma(\nu_e e^- \rightarrow \nu_e e^-)/dT_e) dE}{\int_{10.25 \text{ MeV}}^{14.4 \text{ MeV}} n(E) (r'_\nu + (1 - r'_\nu)P(\nu_e \rightarrow \nu_e; R_0, E)) (d\sigma(\nu_e e^- \rightarrow \nu_e e^-)/dT_e) dE}, \quad (15)$$

where $dN_{\text{ev}}(\Delta m^2, \theta, T_e; k)/dT_e$ is the number of events (observed in k years) with the recoil e^- having an energy T_e , $d\sigma(\nu_e e^- \rightarrow \nu_e e^-)/dT_e$ is the differential cross-section of the process $\nu_e + e^- \rightarrow \nu_e + e^-$, $r'_\nu = (d\sigma(\nu_\mu e^- \rightarrow \nu_\mu e^-)/dT_e)/(d\sigma(\nu_e e^- \rightarrow \nu_e e^-)/dT_e) \cong (\frac{1}{6} - \frac{1}{7})$, and

¹¹More precisely, induced by the "surviving" ${}^8\text{B}$ electron neutrinos and by the $\nu_{\mu(\tau)}$ neutrinos into which the ${}^8\text{B}$ neutrinos have oscillated.

¹²In ref. [14] (see Fig. 3a) we have shown just the ratio of the e^- spectrum in the case of $\nu_e \leftrightarrow \nu_{\mu(\tau)}$ oscillations, and of the standard e^- spectrum, for four pairs of values of Δm^2 and $\sin^2 2\theta$, chosen from different parts of the intervals (1a) and (1b).

$$w(T_e) = \frac{\int_{10.25 \text{ MeV}}^{14.4 \text{ MeV}} n(E) (d\sigma(\nu_e e^- \rightarrow \nu_e e^-)/dT_e) dE}{T_e(1 + \frac{m_e}{2T_e}) \int_{10.25 \text{ MeV}}^{14.4 \text{ MeV}} n(E) (d\sigma(\nu_e e^- \rightarrow \nu_e e^-)/dT_e) dE}. \quad (16)$$

Thus, in the absence of deformations (no reduction, or energy independent reduction of the ${}^8\text{B}$ electron neutrino flux) the double ratio of e^- -spectra (15) will represent a horizontal line crossing the vertical axis at the point 1.

Let us note that one can choose to normalize the ratios of the predicted and the standard spectra discussed above by their values not at 10 MeV, but at some other (in general, different for SNO and Super Kamiokande detectors) energies. For a given experiment the energy of normalization must be chosen on the basis of considerations of accuracy of the corresponding data, and of maximal enhancement of the effect of deformation if present in the spectrum.

One can utilize an alternative spectrum normalization based on the measurement of the total (average) flux of ${}^8\text{B}$ neutrinos with energy $E \geq E_{th}$ to form a solar model independent observable. In the case of the SNO detector this total flux is given by

$$\Phi_B(\Delta m^2, \theta, E_{th}) = \int_{E_{th}}^{14.4 \text{ MeV}} dE \frac{d\Phi_B(\Delta m^2, \theta, E)}{dE}, \quad (17)$$

where the integrand is determined by eq. (11). In the absence of vacuum oscillations (or MSW transitions) the spectrum of ${}^8\text{B}$ neutrinos having energies $E \geq E_{th}$, whose total flux is $\Phi_B(\Delta m^2, \theta, E_{th})$, will have the form: $d\Phi_B^0(E)/dE = n(E) \Phi_B(\Delta m^2, \theta, E_{th})$. The total flux $\Phi_B(\Delta m^2, \theta, E_{th})$ (or the spectrum $d\Phi_B^0(E)/dE$) can be used to normalize the measured spectrum (11). Thus, instead of the double ratio (14) one can consider solar model independent ratio

$$\begin{aligned} \bar{R}_{sp}^{SNO}(\Delta m^2, \theta, E) &= \frac{1}{\Phi_B(\Delta m^2, \theta, E_{th})} \frac{d\Phi_B(\Delta m^2, \theta, E)}{dE} = \\ &= \frac{(\sigma(\nu_e d \rightarrow e^- pp))^{-1} dN_{ev}(\Delta m^2, \theta, E; k)/dE}{\int_{E_{th}}^{14.4 \text{ MeV}} dE (\sigma(\nu_e d \rightarrow e^- pp))^{-1} dN_{ev}(\Delta m^2, \theta, E; k)/dE} = \\ &= \frac{1}{n'(\Delta m^2, \theta, E_{th})} n(E) P(\nu_e \rightarrow \nu_e; R_0, E), \end{aligned} \quad (18)$$

where

$$n'(\Delta m^2, \theta, E_{\text{th}}) = \int_{E_{\text{th}}}^{14.4 \text{ MeV}} n(E) P(\nu_e \rightarrow \nu_e; R_0, E) dE \quad (19)$$

is the total ${}^8\text{B}$ neutrino flux suppression factor in the case of vacuum oscillations, $0 \leq n'(\Delta m^2, \theta, E_{\text{th}}) \leq 1$. The analogous ratio for the Super Kamiokande detector can be easily derived. There are two advantages in utilizing the normalization described above: i) the corresponding ratios of spectra will be determined experimentally with a higher precision than the double ratios (14) and (15), and ii) it allows a straightforward comparison between the theoretical predictions and the data. For certain values of Δm^2 and $\sin^2 2\theta$ the spectra deformations can be less pronounced in the ratios of the type (18) than in the double ratios (14) and (15), and vice versa. This is illustrated in Figs. 5a and 5b, where we show the ${}^8\text{B}$ neutrino spectra depicted respectively in Figs. 4a and 4b, but normalized in the manner described above, eq. (18).

3. MSW TRANSITIONS: IMPRINTS ON THE SPECTRA

In the case of two-neutrino MSW transitions $\nu_e \rightarrow \nu_{\mu(\tau)}$ or $\nu_e \rightarrow \nu_s$ in the Sun, the solar ν_e survival probability, $P(\nu_e \rightarrow \nu_e; E)$, can be calculated with very high accuracy for $\Delta m^2 \gtrsim 5 \times 10^{-8} \text{ eV}^2$ and $\sin^2 2\theta \gtrsim 10^{-3}$ using the simple analytic expression [32,33]:

$$P(\nu_e \rightarrow \nu_e; E) = \frac{1}{2} + \left(\frac{1}{2} - P'\right) \cos 2\theta_m(t_0) \cos 2\theta. \quad (5)$$

Here

$$P' = \frac{\exp[-\pi r_0 \frac{\Delta m^2}{2p} (1 - \cos 2\theta)] - \exp[-2\pi r_0 \frac{\Delta m^2}{2p}]}{1 - \exp[-2\pi r_0 \frac{\Delta m^2}{2p}]} \quad (6)$$

is the level crossing probability (i.e., the analog of the Landau-Zener probability) for the case of density varying exponentially along the neutrino trajectory in the Sun, $\theta_m(t_0)$ is the neutrino mixing angle in matter [13] in the point of ν_e production in the Sun, and r_0 is the "running" scale height [32,33] (see also [14]), i.e., the scale height calculated at the resonance point. For $\Delta m^2 \gtrsim 5 \times 10^{-8} \text{ eV}^2$ and $\sin^2 2\theta \gtrsim 10^{-3}$ expression (5) allows one to derive MSW predictions for any observable quantity associated with the detection of the solar neutrino

flux, or of its different components, on Earth ¹³.

We have re-examined (exploiting the χ^2 -method) the MSW solution of the solar neutrino problem using the most recent published data from all four operating solar neutrino detectors (see Fig. 7). The analysis was based on the SSM predictions of ref. [5]. It revealed that in the case of $\nu_e \rightarrow \nu_{\mu(\tau)}$ transitions i) the "lower" (in values of Δm^2) branch of the large mixing angle (adiabatic) solution [14] (actually, the region $\Delta m^2 < \times 10^{-6} \text{ eV}^2$, $\sin^2 2\theta > 0.1$) is excluded by the current data at 99.5% C.L., ii) the "upper" branch [14] provides a not very good quality of the fit of the data ($\min \chi^2 = 5.30$ (with the theoretical uncertainties included in the analysis) for 2 d.f.), being excluded at 90% C.L., but allowed at 95% C.L., and iii) the small mixing angle (nonadiabatic) solution [14] provides the best fit of the data ($\min \chi^2 = 0.48$ (with the theoretical uncertainties included in the analysis) for 2 d.f.). The results are quite different if one assumes that $\nu_e \rightarrow \nu_s$ transitions take place: in this case only a small mixing angle (nonadiabatic) solution is acceptable (at 90% C.L.: $\min \chi^2 = 3.43$ (without the inclusion of the theoretical uncertainties in the analysis) for 2 d.f.), while a large mixing angle solution is excluded at 99.7% C.L. Note, however, that the nonadiabatic solution in the case of $\nu_e \rightarrow \nu_{\mu(\tau)}$ transitions gives a better quality of the fit of the data than the nonadiabatic solution associated with the $\nu_e \rightarrow \nu_s$ transitions. Our results are presented graphically in Figs. 7, where the regions of values of Δm^2 and $\sin^2 2\theta$, allowed at 90% C.L. and 95% C.L. are depicted: Figs. 7a, 7c and Figs. 7b, 7d correspond respectively to $\nu_e \rightarrow \nu_{\mu(\tau)}$ and $\nu_e \rightarrow \nu_s$ conversions.

The distortions of the spectrum of the ^8B neutrinos ($E \geq 5 \text{ MeV}$) predicted in the

¹³A very precise and simple analytic description of the two-neutrino MSW transitions of solar neutrinos for $\sin^2 2\theta \lesssim 10^{-3}$ was derived in ref. [33]. If $\Delta m^2 \lesssim 5 \times 10^{-8} \text{ eV}^2$, for $\sin^2 2\theta \gtrsim 0.1$ one must take into account in the description of the transitions of the monoenergetic ^7Be and pep neutrinos also the nonadiabatic oscillating term present in $P(\nu_e \rightarrow \nu_e; E)$ [34], for which there exists a relatively simple analytic expression as well [32].

case of two-neutrino MSW transitions are shown in Figs. 4c, 4d, and 5c, 5d, while the corresponding distortions of the spectrum of e^- from the reaction $\nu + e^- \rightarrow \nu + e^-$ induced by the ${}^8\text{B}$ neutrinos are depicted in Figs. 6c and 6d. The MSW spectra shown in Figs. 4c (5c), 4d (5d) and 6c, 6d are normalized in the same way as the vacuum oscillation spectra depicted in Figs. 4a (5a), 4b (5b) and 6a, 6b. Thus, plotted in Figs. 4c (5c), 4d (5d) and 6c, 6d are the corresponding double ratios (14) and (15) (ratio (18)). In previous publications we have shown graphically just the ratio of the predicted MSW and the standard e^- -spectra (ref. [14], Fig. 3b), and the absolute deformations of the ${}^8\text{B}$ and pp neutrino spectra (ref. [27], Fig. 5d) for the same four pairs of values of Δm^2 and $\sin^2 2\theta$, for which Figs. 4c and 6c are obtained. As is evident from Figs. 4–6, the measurements of the ${}^8\text{B}$ neutrino and of the recoil-electron spectra in SNO, Super Kamiokande and ICARUS experiments will allow one, in particular, to discriminate between the MSW nonadiabatic and the MSW adiabatic solutions of the solar neutrino problem.

4. DISTINGUISHING BETWEEN THE VACUUM OSCILLATION AND THE MSW SOLUTIONS

An unambiguous evidence of vacuum oscillations of solar neutrinos would be the observation of clear deviations from the standard 7% seasonal variation of the signals in the future solar neutrino detectors: no other solution of the solar neutrino problem leads to such an effect. In the case of vacuum oscillations the predicted nonstandard seasonal changes of the signals due to the monoenergetic ${}^7\text{Be}$ and pep neutrinos are the most dramatic (see Figs. 1 and 2). Although much smaller, the seasonal variation effects in the signals generated by the ${}^8\text{B}$ neutrinos are, for most of the values of Δm^2 and $\sin^2 2\theta$ from the intervals (1a) and (1b), sufficiently large to be detected by the SNO, Super Kamiokande and ICARUS experiments, provided the detectors will operate with their envisaged detection capabilities and expected background levels. As we have demonstrated, the effects can be enhanced by choosing appropriate values of the relevant threshold detection energies. The data on the seasonal time variations of the event rates in SNO, Super Kamiokande and ICARUS experiments can be

crucial for discriminating between the vacuum oscillation and the other possible solutions of the solar neutrino problem.

The predicted distortions of the ${}^8\text{B}$ neutrino and the recoil-electron spectra due to two-neutrino vacuum oscillations or MSW transitions of the ${}^8\text{B}$ neutrinos (Figs. 4, 5 and 6) provide us with an indispensable possibility to test these solutions in a solar model independent way in SNO, Super Kamiokande and ICARUS experiments. As is evident from the comparison of Figs. 4a,...,4d (5a,...,5d) and Figs. 6a,...,6d, respectively, both the vacuum oscillations and the MSW transitions lead to somewhat stronger shape deformations of the ${}^8\text{B}$ neutrino spectrum than of the recoil-electron spectrum: some of the features of the distorted ${}^8\text{B}$ neutrino spectrum are less pronounced, or are not present, in the e^- spectrum as a result of the integration over the neutrino energy necessary to perform to obtain the latter. The only exception are the spectra corresponding to large mixing angle MSW transitions (see the curves labelled 2 and 3 (4 and 5) in Figs. 4c, 5c and 6c (Figs. 4d, 5d and 6d)). The predicted spectra deformations in this case are rather small and, most probably, will be difficult to detect in SNO, Super Kamiokande and ICARUS experiments. Let us add that the distortions of the spectra can be enhanced by an appropriate choice of the specific normalization of the spectra, with the help of which one forms solar model independent spectrum observables (as a comparison of Figs. 4 and 5 indicates). The results depicted in Figs. 4 and 5 show that the vacuum oscillations, the MSW adiabatic, and the MSW nonadiabatic transitions of solar neutrinos lead to distinctly different deformations of the spectrum of the ${}^8\text{B}$ neutrinos, to be measured in the SNO (ICARUS) experiment. It seems very likely that the data from the SNO (ICARUS) detector on the ${}^8\text{B}$ neutrino spectrum will allow one to test and to discriminate between these three possibilities. Adding the information about the seasonal variations of the signal will, most probably, permit to unambiguously distinguish between the vacuum oscillation and the MSW solutions.

The distortions of the recoil-electron spectrum shown in Figs. 6 suggest that on the basis of the Super Kamiokande (ICARUS) data on the e^- spectrum alone it may be difficult to discriminate between vacuum oscillations with $4.5 \times 10^{-11} \text{eV}^2 \lesssim \Delta m^2 \lesssim 6.3 \times 10^{-11} \text{eV}^2$ and

MSW nonadiabatic transitions of solar neutrinos (compare curves 5 and 6 in Fig. 6a, and 2–5 in Fig. 6b with curves 4 in Fig. 6c and 1–3 in Fig. 6d). In the case of vacuum oscillations with Δm^2 from the above interval there will be seasonal variations of the signals in the Super Kamiokande, SNO and ICARUS detectors (see the dotted, dashed and long-dashed curves in Figs. 3d, 3e and 3f), which can be used to eliminate one of these two possibilities.

It is also clear from Figs. 4, 5 and 6 that the information about the shapes of the ^8B neutrino and the e^- spectra to be obtained in the SNO, Super Kamiokande and ICARUS experiments, most probably, will not be sufficient to discriminate between an astrophysical and the large mixing angle (adiabatic) MSW solutions of the solar neutrino problem. However, the measurement of the ratio of the number of events due to the solar neutrino induced charged current (CC) and neutral current (NC) reactions on deuterium, $R^{CC/NC}$, to be performed with a relatively high precision in SNO experiment, will provide a crucial test of the large mixing angle MSW solution: for this solution one has $R_{AS}^{CC/NC} \cong (0.3 - 0.4) R^{CC/NC}$, where $R^{CC/NC}$ is the value of the ratio predicted in the absence of oscillations and/or of MSW transitions. Note that the quantity $R^{CC/NC}$ does not depend on the total flux of ^8B neutrinos, and therefore is solar model independent; the value of $R^{CC/NC}$ can be calculated with a high precision.

To conclude, the envisaged capabilities of the next generation of solar neutrino experiments will allow one to perform crucial solar model independent tests of, and to discriminate between, the vacuum oscillation and the MSW solutions of the solar neutrino problem. It is very likely that the "solar neutrino puzzle" will be resolved by these experiments.

Acknowledgements.

The kind hospitality and partial support of the Institute for Nuclear Theory at the University of Washington in Seattle, where part of the present work was done, is acknowledged with gratefulness. The work of P.I.K. has been supported by grant No. DE-FG05-85ER-40219 of the U.S. Department of Energy and by a grant from the North Carolina Supercomputing Program.

REFERENCES

- [1] A.I. Abazov et al. (SAGE collaboration), *Phys. Rev. Lett.* 67 (1991) 332; V. Gavrin, Talk given at the XXVIth Int. Conference on High Energy Physics, August 5 - 13, 1992, Dallas (U.S.A.); for latest results see: V.N. Gavrin et al., *Nucl. Phys. B (Proc. Suppl.)* 35 (1994) 412.
- [2] P. Anselmann et al., (GALLEX collaboration), *Phys. Lett.* 285B (1992) 376; the latest results were published in: *Phys. Lett.* 327B (1994) 377 (see also *ibid.* 314B (1993) 445).
- [3] R. Davis, Talk given at the 6th Int. Workshop on Neutrino Telescopes, February 22-24, 1994, Venice; K. Lande et al., *Proc. XXIth Int. Conf. on High Energy Physics, Singapore* (eds. K.K. Phua and Y. Yamaguchi, World Scientific, Singapore, 1991), p. 667.
- [4] J.N. Bahcall and R.K. Ulrich, *Rev. Mod. Phys.* 60 (1988) 298.
- [5] J.N. Bahcall and M. Pinsonneault, *Rev. Mod. Phys.* 64 (1992) 85.
- [6] S. Turck-Chièze et al., *Astrophys. J.* 335 (1988) 425; S. Turck-Chièze and I. Lopes, *Astrophys. J.* 408 (1993) 347.
- [7] A. Suzuki, KEK-preprint-93-96, August 1993; for the results of the Kamiokande-II experiment see: K.S. Hirata et al., *Phys. Rev. Lett.* 65 (1990) 1297 and 1301, *ibid.* 66 (1991) 9.
- [8] J.N. Bahcall and H. Bethe, *Phys. Rev.* D47 (1993) 1298; V. Castellani, S. Degl'Innocenti and G. Fiorentini, *Astron. and Astroph.* 271 (1993) 601; N. Hata and P. Langacker, *Phys. Rev.* D49 (1994) 3622.
- [9] A. Dar and G. Shaviv, Technion preprint Ph-94-5 (1994).
- [10] J.N. Bahcall et al., Institute for Advanced Studies preprint IASSNS-AST 94/13, Princeton, April 1994; A. Yu. Smirnov, Institute for Nuclear Theory preprint INT 94-13-01, Seattle, April 1994; V. Castellani et al., Report INFNFE-3/94; A. Dar and G. Shaviv,

Technion preprint ASTRO-PH-9404035, April 1994.

- [11] B. Pontecorvo, Zh. Eksp. Teor. Fiz. 33 (1957) 549; *ibid.* 34 (1958) 247; *ibid.* 53 (1967) 1717; Z. Maki, M. Nakagawa and S. Sakata, Prog. Theor. Phys. 28 (1962) 870.
- [12] P.I. Krastev and S.T. Petcov, Phys. Lett. 285B (1992) 85; *ibid.* 299B (1993) 99.
- [13] S.P. Mikheyev and A.Yu. Smirnov, Yad. Fiz. 42 (1985) 1441; L. Wolfenstein, Phys. Rev. D17 (1978) 2369.
- [14] P.I. Krastev and S.T. Petcov, Phys. Lett. 299B (1993) 99.
- [15] X. Shi, D.N. Schramm, and J.N. Bahcall, Phys. Rev. Lett. 69 (1992) 717; L.M. Krauss, E. Gates and M. White, Phys. Lett. 299B (1993) 95; A. Bludman et al., Phys. Rev. D47 (1993) 2220; N. Hata and P. Langacker, Phys. Rev. D48 (1993) 2937; G. Fiorentini et al., Report INFNFE-10/93.
- [16] C.-S. Lim and W. Marciano, Phys. Rev. D37 (1988) 1368; E.Kh. Akhmedov, Phys. Lett. 213B (1988) 64.
- [17] P.I. Krastev, Phys. Lett. 303B (1993) 75; E.Kh. Akhmedov, A. Lanza and S.T. Petcov, Phys. Lett. 303B (1993) 85.
- [18] M.M. Guzzo, A. Masiero and S.T. Petcov, Phys. Lett. 260B (1991) 154; M.M. Guzzo and S.T. Petcov, Phys. Lett. 271B (1991) 172.
- [19] E. Roulet, Phys. Rev. D44 (1991) R935.
- [20] J.N. Bahcall, N. Cabibbo and A. Yahil, Phys. Rev. Lett. 28 (1972) 316; J.N. Bahcall et al., Phys. Lett. 181B (1986) 369; J. Frieman, H. Haber and K. Freese, Phys. Lett. 200B (1988) 115.
- [21] Z.G. Berezhiani et al., Z. Phys. C54 (1992) 581.
- [22] G. Ewan et al., Sudbury Neutrino Observatory Proposal, SNO-87-12, 1987; G. Aardsma

- et al., Phys. Lett. 194B (1987) 321.
- [23] T. Kajita, Physics with the Super Kamiokande Detector, ICRR Report 185-89-2, 1989.
- [24] C. Arpesella et al., BOREXINO proposal (eds. G. Bellini, R. Raghavan et al., Univ. of Milano, Milano 1992), vols. 1 and 2.
- [25] J.N. Bahcall, M. Baldo-Ceolin, D. Cline, and C. Rubbia, Phys. Lett. 178B (1986) 324; ICARUS collaboration, "ICARUS I: An Optimized, Real Time Detector of Solar Neutrinos", Frascati report LNF-89/005(R), 1989.
- [26] G. Laurenti et al., Proc. of the 5th Int. Workshop on Neutrino Telescopes, March 2-4, 1993, Venice (ed. M. Baldo-Ceolin), p. 161.
- [27] P.I. Krastev and S.T. Petcov, reported by S.T. Petcov in Proc. of the 5th Int. Workshop on Neutrino Telescopes, March 2-4, 1993, Venice (ed. M. Baldo-Ceolin), p. 23.
- [28] J.N. Bahcall, Phys. Rev. D44 (1991) 1644.
- [29] S.M. Bilenyk and C. Giunti, Phys. Lett. 311B (1993) 179; *ibid* 320B (1994) 323.
- [30] P.I. Krastev and S.T. Petcov, Phys. Rev. Lett. 72 (1994) 1960; preprint IFP-480-UNC/SISSA 177/93/EP (Updated Version), March 1994 (to be published in the Proc. of the 6th Int. Workshop on Neutrino Telescopes, February 22-24, 1994, Venice).
- [31] S.M. Bilenyk and B. Pontecorvo, Phys. Rep. 41 (1978) 225.
- [32] S.T. Petcov, Phys. Lett. 200B (1988) 373; *ibid*. 214B (1988) 139; see also: Nucl. Phys. B (Suppl.) 13 (1990) 527.
- [33] P.I. Krastev and S.T. Petcov, Phys. Lett. 207B (1988) 64; (E): *ibid*. 214B (1988) 661; Proc. of the Moriond Workshop "5th Force, Neutrino Physics", January 1988, Les Arcs (eds. O. Fackler and J. Tran Thanh Van, Frontières, Gif-sur-Yvette, 1988), p. 179.
- [34] J. Rich and S.T. Petcov, Phys. Lett. 224B (1989) 426. (1993) 2369.

Figure Captions

Fig. 1 The ratio of the vacuum oscillation ($\nu_e \leftrightarrow \nu_{\mu(\tau)}$) and of the SSM predicted signals (event rates) due to the ^8B , pep, ^7Be , and pp neutrinos as a function of the time of the year (in units of 365 days). The results shown are for experiments detecting the solar neutrinos via the $\nu - e^-$ elastic scattering reaction (Super Kamiokande, BOREXINO, HELLAZ, etc.). The SSM predicted signals used represent the time independent one year average values of the event rates calculated within the model [5].

Fig. 2 The same as in Fig. 1 for different sets of values of Δm^2 and $\sin^2 2\theta$. Figures e and f correspond to $\nu_e \leftrightarrow \nu_s$ oscillations.

Fig. 3 Time variations of the signals in Super Kamiokande (Figs. 3a, 3b, 3d and 3e) and SNO (Figs. 3d and 3f) detectors in the case of vacuum oscillations of ^8B neutrinos, for the same values of the parameters Δm^2 and $\sin^2 2\theta$ for which Figs. 1a, 1b,..., 1f and Figs. 2a, 2b,..., 2f have been obtained (solid, dotted, dashed, long-dashed, dash-dotted and long-dash-dotted lines in Figs. 3a-3c and 3d-3f, respectively). The signals are normalized in such a way that in the absence of deviations from the standard 7% seasonal variation they will be constant in time and equal to 1 (i.e., horizontal lines crossing the vertical axis at the point 1); the normalization used renders solar model independent the ratio of signals plotted. The results presented in Fig. 3a (3d) and Fig. 3b (3e) have been obtained with different values of the neutrino threshold energy: $E_{th} = 5$ MeV and $E_{th} = 7.5$ MeV, respectively.

Fig. 4 Deformations of the ^8B neutrino spectrum in the cases of $\nu_e \leftrightarrow \nu_{\mu(\tau)}$ (or $\nu_e \leftrightarrow \nu_s$) oscillations (a and b), and of $\nu_e \rightarrow \nu_{\mu(\tau)}$ (or $\nu_e \rightarrow \nu_s$) MSW transitions (c and d). The vacuum oscillation and the MSW spectra are divided by the SSM predicted spectrum [5], and each ratio of spectra is further normalized to the value this ratio has at $E = 10$ MeV. The double ratios plotted are solar model independent quantities.

Fig. 5 The same as in Fig. 4, but with different normalization of the spectra (see eq. (18)).

Fig. 6 Deformations of the spectrum of e^- from the reaction $\nu + e^- \rightarrow \nu + e^-$ caused

by ${}^8\text{B}$ neutrinos, in the cases of oscillations in vacuum $\nu_e \leftrightarrow \nu_{\mu(\tau)}$ (a, and b (curves 1-4)), $\nu_e \leftrightarrow \nu_s$ (b (curves 5 and 6)), and of MSW transitions $\nu_e \rightarrow \nu_{\mu(\tau)}$ (c and d). Each of the predicted recoil-electron spectrum is divided by the standard one and the ratio so obtained is normalized to the value it has at $T_e = 10$ MeV.

Fig. 7 Regions of values of the parameters Δm^2 and $\sin^2 2\theta$ allowed at 90% C.L. (dashed lines) and at 95% C.L. (solid lines) by the current solar neutrino data in the case of MSW $\nu_e \rightarrow \nu_{\mu(\tau)}$ (a and c) and $\nu_e \rightarrow \nu_s$ (b and d) transitions of solar neutrinos. Figures a and b (c and d) have been obtained by including (without including) the uncertainties in the theoretical predictions [5] in the relevant χ^2 - analysis.

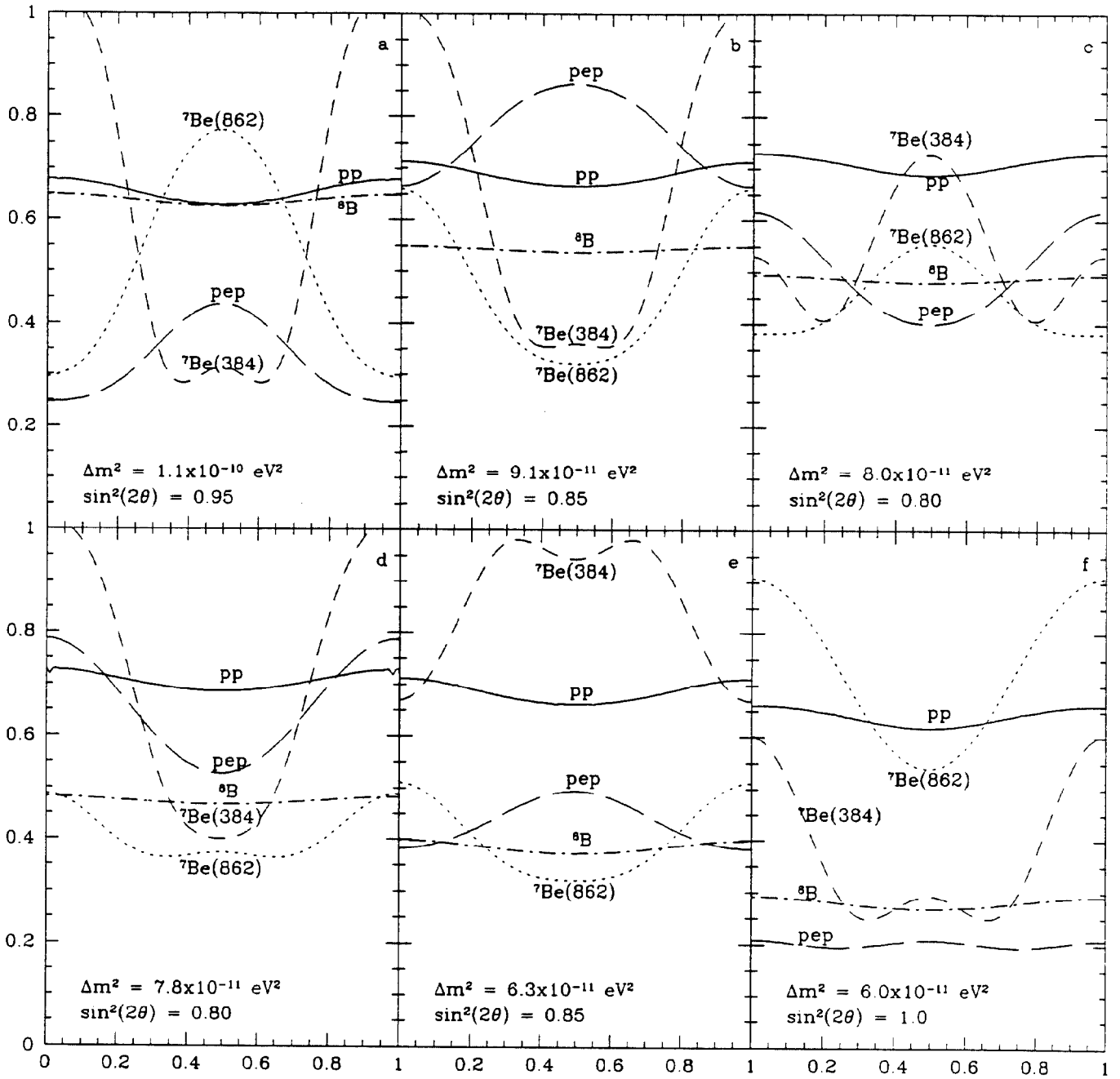


Fig.1

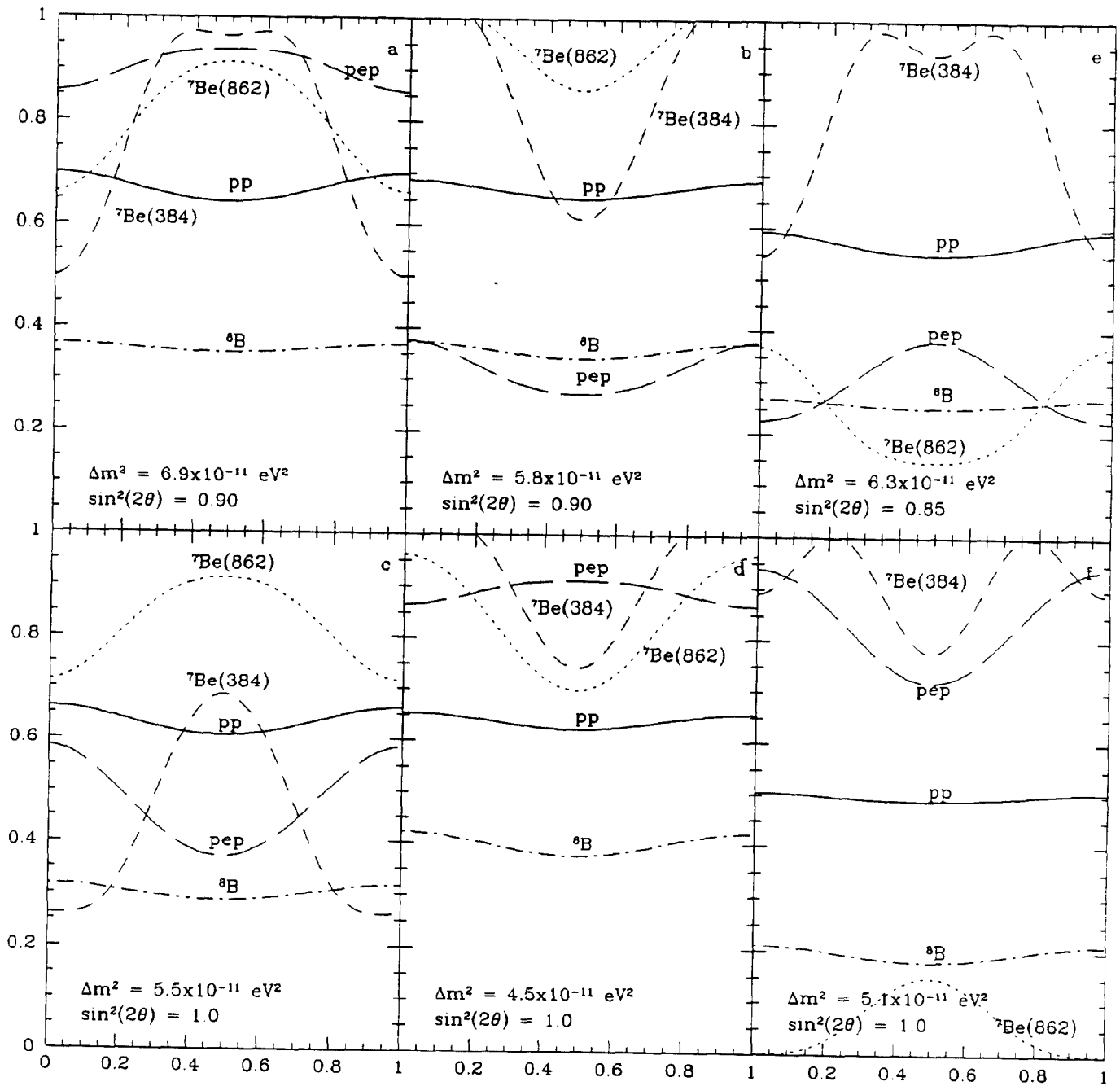


Fig.2

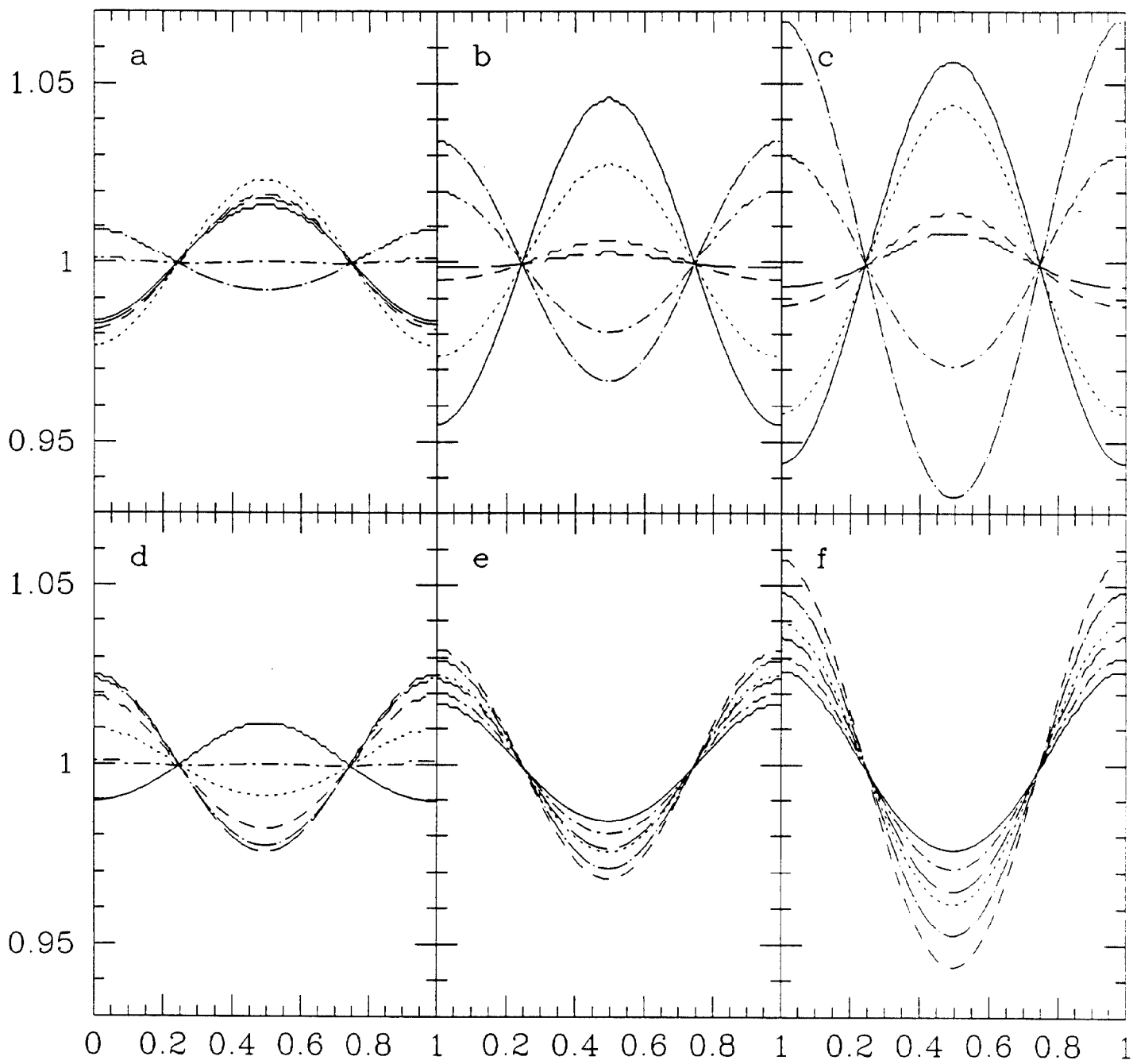


Fig.3

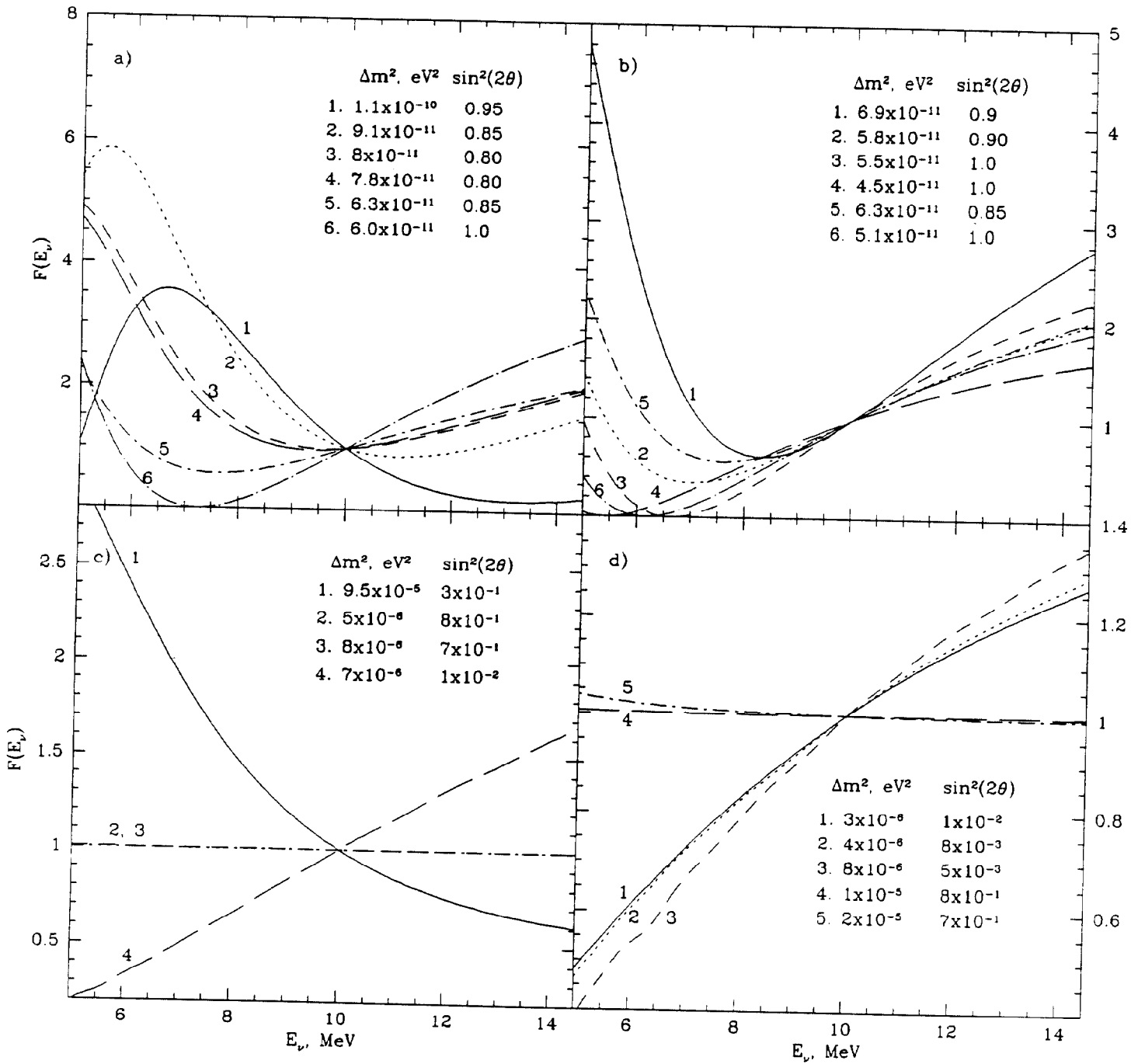


Fig.4

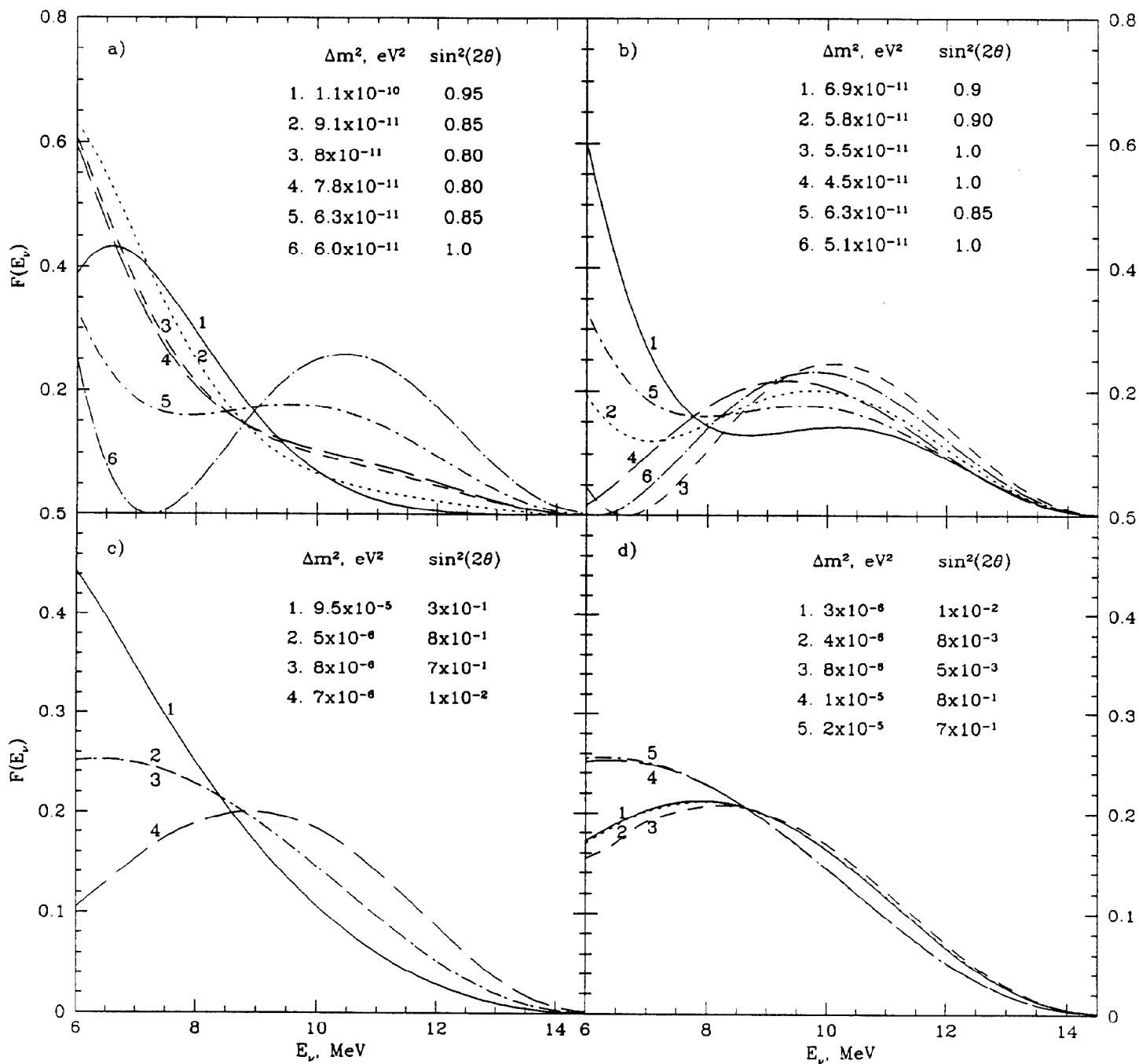


Fig.5

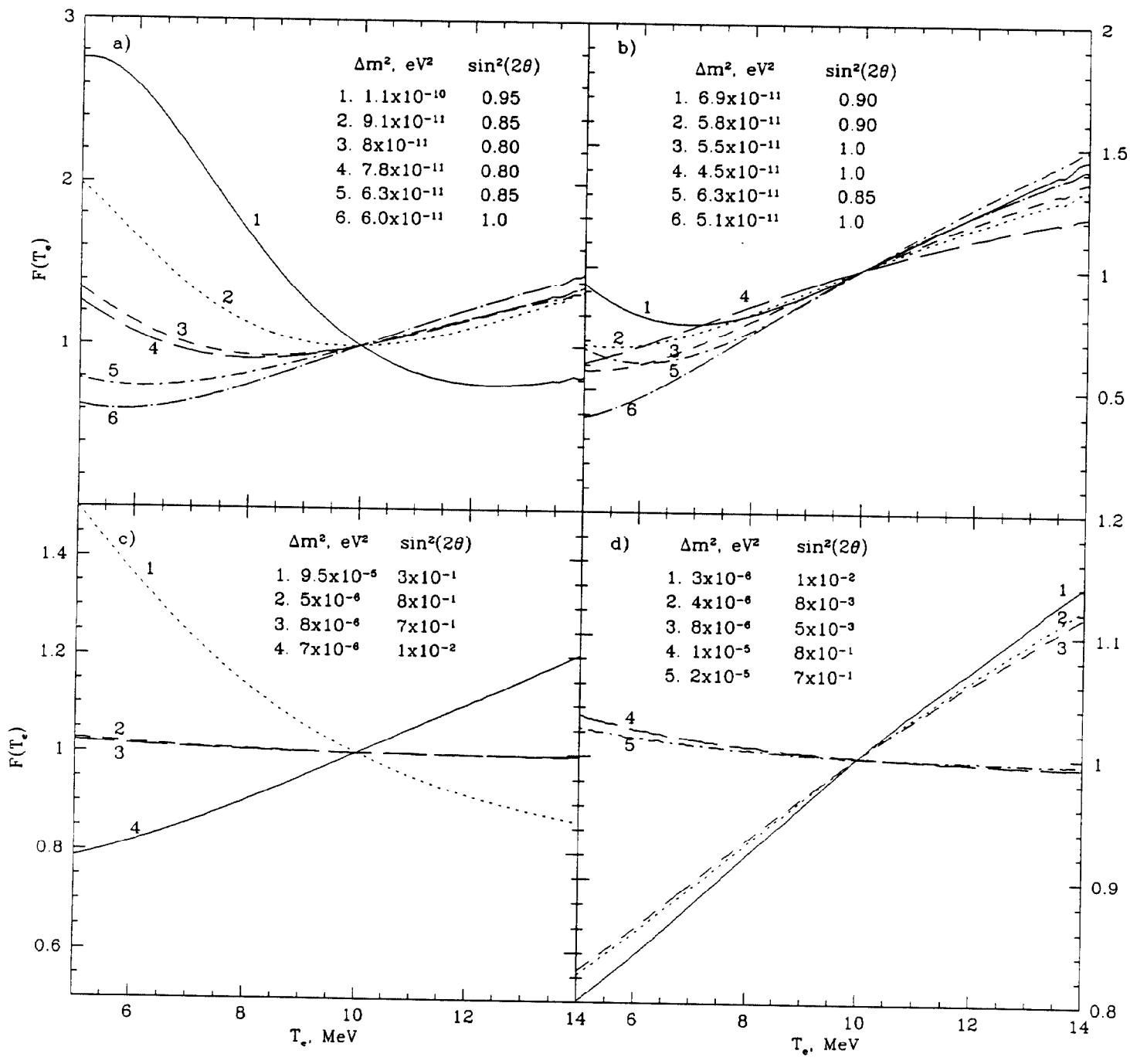


Fig.6

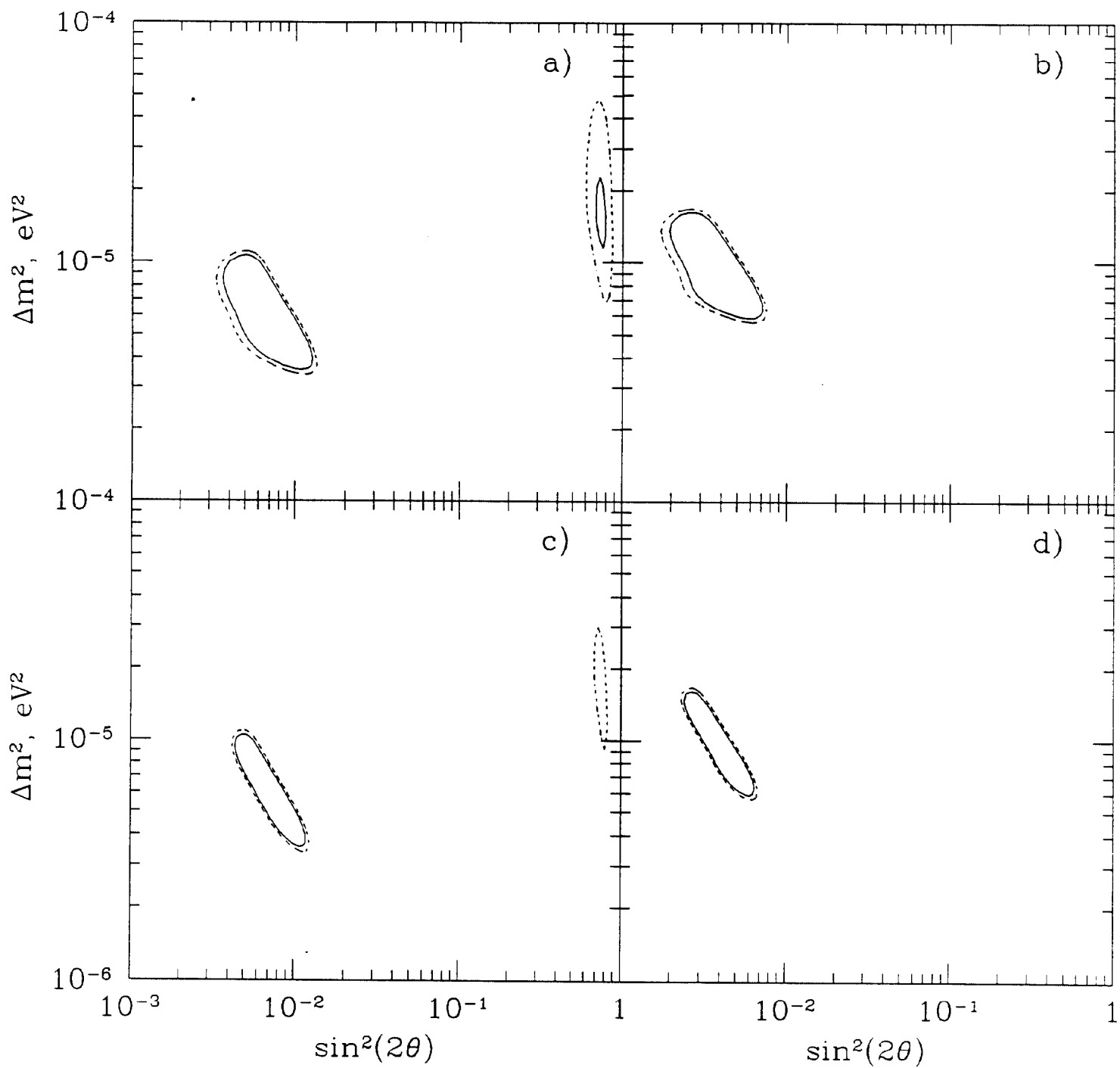


Fig.7